Dyes and Pigments 99 (2013) 67–73

Contents lists available at SciVerse ScienceDirect

Dyes and Pigments

journal homepage: www.elsevier.com/locate/dyepig

# Synthesis and characterization of blue-to-green electrophosphorescence emitter based on pyrazole iridium complexes

Xu Huixia [a,b,*], Yue Yan [c], Qu Litao [c], Hao Yuying [c], Wang Hua [a,b], Chen Liuqing [a,b], Xu Bingshe [a,b]

[a] Key Laboratory of Interface Science and Engineering in Advanced Materials, Ministry of Education, Taiyuan University of Technology, Taiyuan 030024, PR China
[b] Shanxi Research Center of Advanced Materials Science and Technology, Taiyuan 030024, PR China
[c] Department of Physics and Optoelectronics, Taiyuan University of Technology, Taiyuan 030024, PR China

ARTICLE INFO

*Article history:*
Received 2 January 2013
Received in revised form
16 April 2013
Accepted 17 April 2013
Available online 25 April 2013

*Keywords:*
Iridium complex
Triazol
Pyrazole
Electrophosphorescent
Blue-light emitting
Roll-off efficiency

ABSTRACT

To overcome the roll-off efficiency of electrophosphorescent organic light-emitting devices, Ir(III) complexes of $(ppz)_2Ir(NN)$ were synthesized and named for $(ppz)_2Ir(tfmpptz)$, $(ppz)_2Ir(fpptz)$, $(ppz)_2Ir(tfmptz)$ and $(ppz)_2Ir(pybi)$ (ppz: 1-phenylpyrazolato; *NN*: *N*, *N′*-heteroaromatic). Their molecular structures, photophysical properties and cyclic voltammetric data were reported. The crystals of $(ppz)_2Ir(tfmpptz)$, $(ppz)_2Ir(fpptz)$ are monoclinic, space group P2(1)/n, and $(ppz)_2Ir(tfmptz)$ is triclinic, space group P-1. The emission maximum peaks of $(ppz)_2Ir(tfmpptz)$, $(ppz)_2Ir(fpptz)$, $(ppz)_2Ir(tfmptz)$ and $(ppz)_2Ir(pybi)$ at room temperature appear at 486, 497, 473 and 530 nm, respectively. The devices with architecture of ITO/NPB (30 nm)/CBP: $(ppz)_2Ir(NN)$ (6%, 30 nm)/BAlq(10 nm)/$Alq_3$(30 nm)/LiF(1 nm)/Al (100 nm) were fabricated by thermal evaporation. The results indicate that the larger steric hindrance of ancillary ligands efficiently suppressed the roll-off of efficiency at high current density.



## 1. Introduction

Phosphorescent organic light-emitting devices (PhOLEDs) have shown great potential in digital terminal displays and planar solid-state lighting. However, it is difficult to develop high-efficiency blue PhOLEDs because of the roll-off in efficiency at high current density [1–3]. The primary importance in achieving high-efficiency PhOLED is that the density of triplet excitons should be right low for the purpose of minimizing triplet–triplet (T–T) exciton annihilation. This intention can be realized by synthesizing Ir(III) complex with larger steric hindrance to distribute the triplet excitons in the bulk emission layer [4,5]. The well-known blue-light Ir(III) complex, FIrpic (iridium(III) bis(4,6-difluorophenylpyridinato-N, C2′) picolinate) was designed based on the green emission $(ppy)_2Ir(acac)$ (bis(2-phenylpyridine) (acetylacetonate)-iridium(III)) by the introduction of electron-withdrawing fluoro groups to the phenyl ring and the use of pic ligand as the ancillary ligand [4]. The efficiencies of FIrpic-based OLEDs have been improved over the years, but a few critical problems need to be resolved, such as inferior color purity [6,7]. The true-blue *fac*-$Ir(ppz)_3$ (*fac*-tris(1-phenylpyrazolato)iridium(III)) was reported with a $\lambda_{max}$414 nm at 77 K, while it is non-emissive at room temperature as a result of the small activation energy to a non-emissive dd excited state [8]. To obtain room-temperature blue-light phosphorescent emitter, FIrtaz and $FIrN_4$ were reported by substituting pic with triazolate or tetrazolate ligand [9]. However, the efficiency decrease sharply from 7.2 to 1.7 lm/W of device based-on $FIrN_4$ at 100 mA/cm$^2$ of current density. Thus, it is a desirable approach to realize room-temperature blue phosphorescent emitter and avoid the efficiency roll-off by inserting larger steric hindrance *N*, *N′*-heteroaromatic (*NN*) ligands [3,10].

Therefore, in this manuscript, the design and synthesis of a series of $(ppz)_2Ir(NN)$ phosphorescent heteroleptic iridium complexes were described. Their chemical structure and synthetic routs are displayed in Scheme 1.

* Corresponding author. Key Laboratory of Interface Science and Engineering in Advanced Materials, Ministry of Education, Taiyuan University of Technology, Taiyuan 030024, PR China. Tel.: +86 03516014852; fax: +86 0351 6010311.
*E-mail address:* xuhuixia0824@163.com (X. Huixia).

0143-7208/$ – see front matter 
http://dx.doi.org/10.1016/j.dyepig.2013.04.022

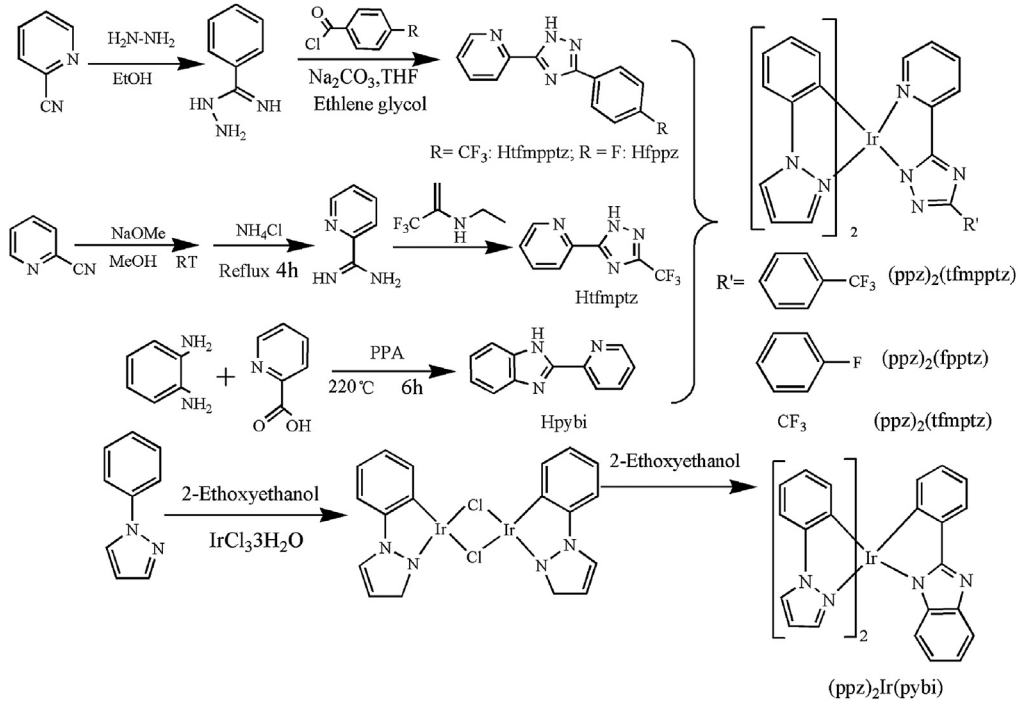


**Scheme 1.** The synthetic routs of $(ppz)_2Ir(NN)$ complexes.

## 2. Experimental section

### 2.1. General information

$^1$H NMR data were recorded with Switzerland Bruker DR × 600 NMR spectrometers. FT-IR spectra were measured with a Nicolet 7199B spectrometer in KBr pellets in the range of 4000–400 cm$^{-1}$. UV–vis absorption spectra were recorded by Lambda Bio 40, American PE Co. The electroluminescent (EL) spectra were measured by PR-655 spectrophotometer. Photoluminescent (PL) spectra were examined by Cary Eclipse fluorescence spectrophotometer in $CH_2Cl_2$ solution. Phosphorescent spectra at 77 K in 2-methyltetrahydrofuran were measured on Hitachi Model F-7000 spectrophotometer upon excitating at the absorption maxima. Cyclic voltammetry was performed with Autolab/PG STAT302 in a one-compartment electrolysis cell using two platinum wires as working electrode and counter, a calomel electrode as reference. $TBAPF_6$ was used as supporting electrolyte (0.1 M). Cyclic voltammetric behaviors were monitored at scan rate 50 mV/s.

To evaluate the electroluminescent properties of these complexes, several electroluminescent devices were fabricated by using $(ppz)_2Ir(NN)$ complexes as dopant emitters. Organic layers were fabricated by high-vacuum ($3 \times 10^{-4}$ Pa) thermal evaporation onto a glass substrate precoated with an indium tin oxide (ITO) layer. The device structure was ITO/NPB (30 nm)/CBP: $(ppz)_2Ir(NN)$ complexes (6%, 30 nm)/BAlq(10 nm)/$Alq_3$(30 m)/LiF(1 nm)/Al (100 nm). Materials used for the device were NPB (N, *N*′-Bis (naphthalen)-N, *N*′-bis (phenyl)-benzidine) for hole-transport layer, $(ppz)_2Ir(NN)$ (6%) in CBP (4,4′-*N*,*N*′-dicarbazolebiphenyl) for light-emitting layer, BAlq (aluminum (III) bis (2-methyl-8-quninolinato)-4-phenylphenolate) for hole-blocking layer, and $Alq_3$ (tris(8-hydroxyquinoline) aluminum) for electron-transport layer. The voltage–current density (V-J) characteristics of PhOLEDs were recorded on Keithley 2400 Source Meter and L-2188 Spot Brightness Meter.

X-ray single-crystal diffractions of all complexes were performed on Bruker SMART APEX II diffractometer with Mo Ka radiation ($\lambda = 0.710\ 73$ Å). The structures were solved with direct methods (SHELX-97) and refined with full-matrix least-squares technique. All non-hydrogen atoms were refined anistropically and hydrogen atoms of organic ligands were geometrically placed.

### 2.2. Theoretical methodology

All calculations were performed using Gaussian 03 package by employing experimental parameters determined by X-ray single-crystal diffraction as input file. The geometry optimization of ground state were carried out using B3LYP functional with 6-31G(d) basis sets [11,12], except for LANL2DZ basis sets for Ir atom. The theoretical absorption spectra were calculated by time-dependent density functional theory (TD-DFT) method [13,14] based on the optimized ground-state structures with solvent effects take into account by the polarizable continuum model (PCM) [15]. Dichloromethane ($CH_2Cl_2$) was chosen as to be consistent with experimental conditions.

## 3. Synthesis of ligand

*Procedure for the synthesis of 2-(5-(4-(trifluoromethyl)phenyl)-2H-1,2,4-triazol-3-yl)pyridine (Htfmpptz)*: A mixture of picolinonitrile (50 mmol), hydrazine hydrate (50 mmol) and ethanol (25 ml) was reacted for 8 h under nitrogen air. The redundant ethanol was removed at room temperature by vacuum. The residue was washed using ether. A white crystal of (2-pyridine) amidrazone was filtered and dried. Then, (2-pyridine)amidrazone (30 mmol), $Na_2CO_3$ (30 mmol) and 4-(trifluoromethyl)benzoyl chloride (30 mmol) in THF solution were reacted for 6 h at room temperature under nitrogen air. The resulting residue was recrystallized in ethanol. The needle-like crystal of 2-(5-(4-

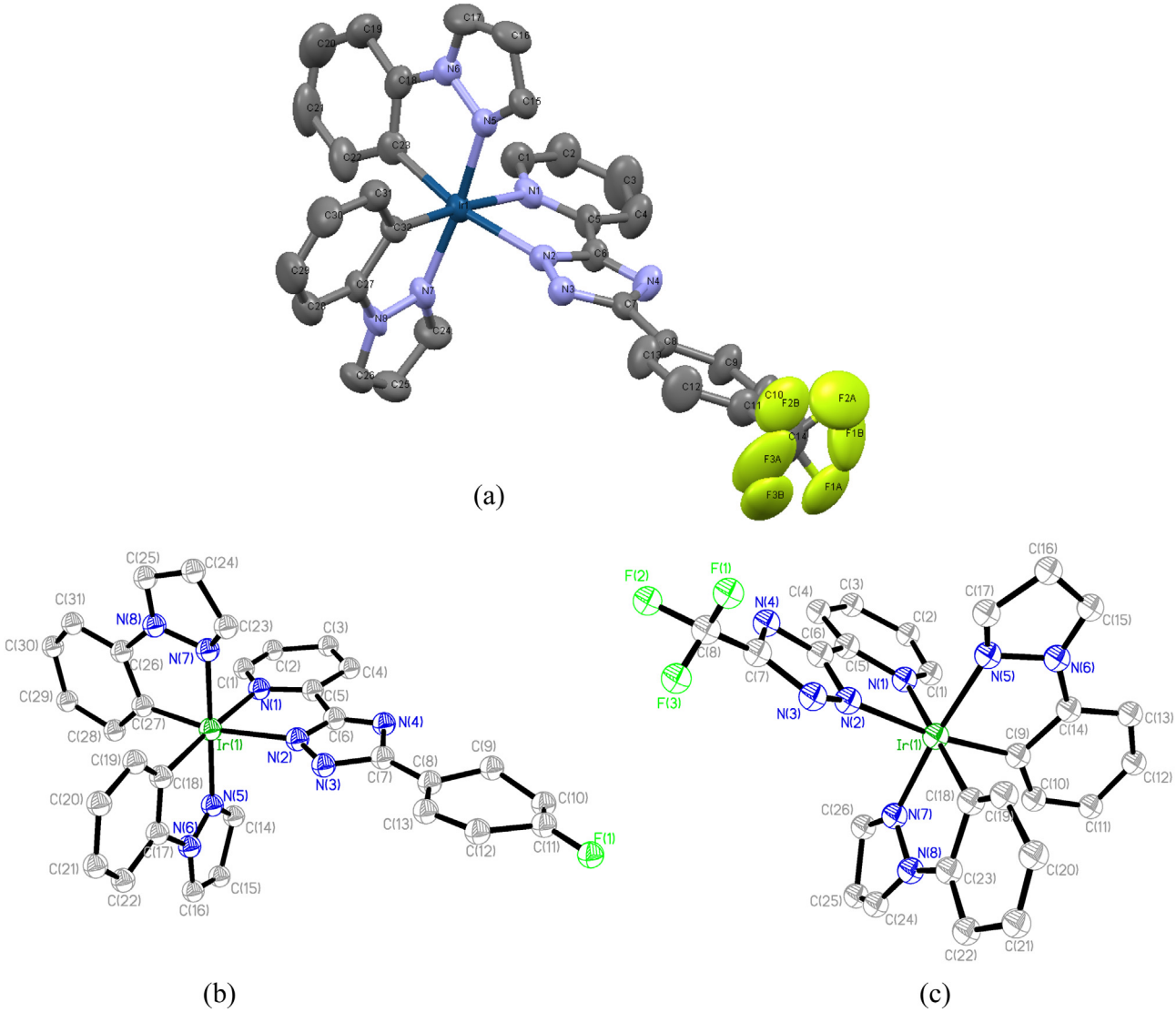


**Fig. 1.** ORTEP diagrams of $(ppz)_2Ir(tfmpptz)$ (a) $(ppz)_2Ir(fpptz)$ (b) and $(ppz)_2Ir(tfmptz)$ (c) with thermal ellipsoid show at 30% probability level; (Selected bond distances of $(ppz)_2Ir(tfmpptz)$: Ir(1)-N(1) = 2.176(5), Ir(1)-N(2) = 2.131(5), Ir(1)-N(5) = 2.016(5), Ir(1)-N(7) = 2.042(5), Ir(1)-(C32) = 1.997(6), Ir(1)-(C23) = 2.010(6) Å; Selected bond distances for $(ppz)_2Ir(fpptz)$: Ir(1)-N(1) = 2.163(5), Ir(1)-N(2) = 2.125(6), Ir(1)-N(5) = 2.015(5), Ir(1)-N(7) = 2.021(5), Ir(1)-C(18) = 1.964(8), Ir(1)-C(27) = 2.035(6) Å; Selected bond distances for $(ppz)_2Ir(tfmptz)$: Ir(1)-N(1) = 2.145(4), Ir(1)-N(2) = 2.108(4), Ir(1)-N(5) = 2.016(4), Ir(1)-N(7) = 2.026(5), Ir(1)-C(18) = 2.013(5), Ir(1)-C(9) = 2.015(5) Å.).

(trifluoromethyl)phenyl)-2H-1,2,4-triazol-3-yl)pyridine was obtained. Yield: 80%. $^1$H NMR (600 MHz, DMSO): $\delta$ 15.08(1H, s), 8.76(1H, d), 8.31(2H, d), 8.20(1H, d), 8.05(1H, t), 7.88(2H, d), 7.58(1H, s); FT-IR (KBr) cm$^{-1}$: 3083, 1631, 1470, 1329, 1171, 1113, 1063, 1017, 847, 731.

The synthesis process of 2-(5-(4-fluorophenyl)-2H-1, 2, 4-thiazol-3-yl)pyridine (Hfpptz) was similar with that of Htfmpptz. Yield: 80%. $^1$H NMR (600 MHz, DMSO): $\delta$ 14.87(1H, s), 8.74(1H, d), 8.18(1H, d), 8.14–8.12(2H, m), 8.04(1H, t), 7.57(1H, dt), 7.34(2H, ddd); FT-IR (KBr) cm$^{-1}$: 3075, 1606, 1465, 1420, 1212, 1158, 1017, 856, 756, 619.

*Procedure for the synthesis of 2-(5-(trifluoromethyl)-2H-1, 2, 4-triazol-3-yl)pyridine (Htfmptz)*: Picolinonitrile and sodium methoxide (10:1) resolved in methanol was stirred under nitrogen at room temperature for 12 h. Then, $NH_4Cl$ was added. After stirred at room temperature for 16 h, the mixture was heated to reflux for 4 h. The solvent was removed at room temperature by vacuum. The product was washed in ether for many times in order to remove residual $NH_4Cl$. 2-Iminazole pyridine hydrochloride were obtained.

Ethyl trifluoroacetate and hydrazine hydrate (1:1.2) were added in anhydrous THF (30 ml) and the mixture was stirred at room temperature for 12 h. The equiv of NaOH with 2-iminazole pyridine hydrochloride (1:1) were added in above-mentioned solution and heated to reflux for 12 h. Sodium carbonate was used to adjust pH value. The solution was extracted into ethyl acetate, which was combined, dried over $MgSO_4$. The residue was subjected to silica gel column chromatography using a 1:3 mixture of ethyl acetate and hexane as the eluent and crystallized in ethyl acetate. The white crystals were obtained. Yield: 80%. $^1$H NMR (600 MHz, $CDCl_3$): $\delta$ 14.05(1H, dr), 8.84(1H, d), 8.35(1H, d), 7.99(1H, dt), 7.55(1H, ddd); FT-IR (KBr) cm$^{-1}$: 3137 1606, 1494, 1461, 1428, 1217, 1189, 1009, 765, 714.

*Procedure for the synthesis of 2-(pyridin-2-yl)-1H-benzo[d]imidazole (Hpybi)*: Benzene-1, 2-diamine and picolinic acid were heated to 220 °C using polyphosphoric acid (PPA) as catalyst, as described in Ref. [16]. $^1$H NMR (600 MHz, DMSO): $\delta$ 13.09(1H, s), 8.74(1H, d), 8.33(1H, dd), 8.01(1H, dt), 7.71(1H, d), 7.52–7.55 (2H, m), 7.26–7.20(2H, m); FT-IR (KBr) cm$^{-1}$: 3322, 3245, 3054, 1593, 1492, 1417, 1319, 1259, 1130, 1037, 840, 798, 734, 522, 468.

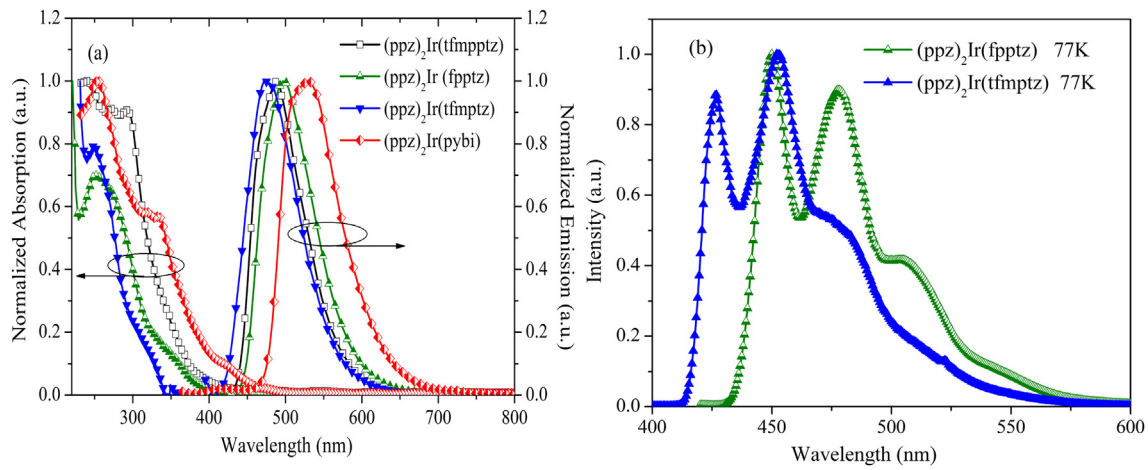


**Fig. 2.** The absorption and PL spectra of all complexes at room temperature in $CH_2Cl_2$ (a) and phosphorescence spectra of $(ppz)_2Ir(fpptz)$ and $(ppz)_2Ir(tfmptz)$ at 77 K in 2-methyltetrahydrofuran (b).

## 4. Synthesis of complexes

Iridium trichloride hydrate in 2-ethoxyethanol was treated with 2, 5-dihydro-1-phenyl-1H-pyrazole (Hppz) to give the chloride-bridged dimer. Further reaction of the dimmer with the *NN* ligands of Htfmpptz, Hfpptz, Htfmptz and Hpybi afforded complexes $(ppz)_2Ir(tfmpptz)$, $(ppz)_2Ir(fpptz)$, $(ppz)_2Ir(tfmptz)$ and $(ppz)_2Ir(pybi)$, respectively [17].

Spectra data for $(ppz)_2Ir(tfmpptz)$: $^1$H NMR (600 MHz, DMSO): $\delta$ 8.81(1H, d), 8.77(1H, d), 8.17(1H, d), 8.15(1H, s), 8.13(1H, s), 8.05(1H, dt), 7.83(1H, d), 7.570(1H, s), 7.69(1H, s), 7.61(1H, d), 7.58(1H, d),7.38(1H, ddd), 7.05(1H, d), 6.97(1H, dt), 6.91 (1H, dt), 6.88(1H, d), 6.82(1H, dt), 6.70(1H, dt), 6.64(1H, t), 6.60(1H, t), 6.23(1H, dd), 6.17(1H, dd); FT-IR (KBr) cm$^{-1}$: 2029, 1615,1481, 1416, 1333, 1171, 1121, 1067, 860, 756.

Selected single crystal data of $(ppz)_2Ir(tfmpptz)$: $C_{32}H_{22}F_3IrN_8$, $M$ = 767.78, Monoclinic, space group P2(1)/n, $T$ = 296(2) K, $a$ = 12.062(7), $b$ = 16.755(10), $c$ = 17.647(11) Å, $\alpha = \gamma = 90°$, $\beta$ = 102.682(6)°, $V$ = 3479(4) Å$^3$, $Z$ = 4, $\rho_c$ = 1.466 mg/cm$^3$, Crystal size = 0.26 × 0.23 × 0.21 mm$^3$, $F$(0 0 0) = 1496, GOF = 0.984, 19579 independent reflections collected with R(int) = 0.0675, Final R [I > 2σ(I)] = 0.0732, wR$_2$ (all data) = 0.0788.

Spectra data for $(ppz)_2Ir(fpptz)$: $^1$H NMR (600 MHz, DMSO): $\delta$ 8.82(1H, d), 8.78(1H, d), 8.15(1H, d), 8.05(1H, dt), 7.98–7.96 (2H, m), 7.83(1H, d), 7.62(1H, d), 7.59(1H, d), 7.37 (1H, ddd), 7.17 (2H, t), 7.05(1H, d), 6.99(1H, dt), 6.92(1H, dt), 6.88(1H, d), 6.81(1H, dt), 6.71(1H, dt), 6.65(1H, t), 6.61(1H, t), 6.24(1H, dd), 6.18(1H, dd); FT-IR (KBr) cm$^{-1}$: 2029, 1615, 1511, 1482, 1407, 1055, 760, 632.

Selected single crystal data of $(ppz)_2Ir(fpptz)$: $C_{31}H_{22}FIrN_8$, $M$ = 717.77, Monoclinic, space group P2(1)/n, $T$ = 296(2) K, $a$ = 12.079(5), $b$ = 16.556(7), $c$ = 16.459(7) Å, $\alpha = \gamma = 90$, $\beta$ = 102.163(4)°, $V$ = 3218(2) Å$^3$, $Z$ = 4, $\rho_c$ = 1.482 mg/cm$^3$, Crystal size = 0.32 × 0.30 × 0.21 mm$^3$, $F$(0 0 0) = 1400, GOF = 1.096, 19014 independent reflections collected with R(int) = 0.0602, Final R [I > 2σ(I)] = 0.0728, wR$_2$ (all data) = 0.0772.

Spectra data for $(ppz)_2Ir(tfmptz)$: $^1$H NMR (600 MHz, DMSO): $\delta$ 8.81(1H, dd), 8.79(1H, dd), 8.19(1H, d), 8.09(1H, dt), 7.85 (1H, d), 7.62(1H, dd), 7.58(1H, dd), 7.48(1H, ddd), 7.08 (1H, d), 6.99 (1H, dt), 6.91(2H, dt), 6.84(1H, d), 6.81(1H, dt), 6.69(1H, dt), 6.65 (1H, t), 6.63(1H, t), 6.23(1H, dd), 6.14(1H, dd); FT-IR (KBr) cm$^{-1}$: 3129, 1617, 1478, 1420, 1283, 1200, 1121, 1034, 756.

Selected single crystal data of $(ppz)_2Ir(tfmptz)$: $C_{26}H_{18}F_3IrN_8$, $M$ = 691.68, Triclinic, space group P-1, $T$ = 293(2) K, $a$ = 9.259(5), $b$ = 11.956(6), $c$ = 13.730(7) Å, $\alpha$ = 95.760(4), $\beta$ = 99.131(4), $\gamma$ = 108.957(4)°, $Z$ = 2, $\rho_c$ = 1.640 mg/cm$^3$, Crystal size = 0.29 × 0.27 × 0.22 mm$^3$, $F$(0 0 0) = 668, GOF = 1.031, 8972 independent reflections collected with R(int) = 0.0304, Final R [I > 2σ(I)] = 0.0708, wR$_2$ (all data) = 0.0728.

Spectra data for $(ppz)_2Ir(pybi)$: $^1$H NMR (600 MHz, DMSO): $\delta$ 8.80(1H, s), 8.76(1H, s), 8.45(1H, d), 8.14(1H, t), 7.92 (1H, d), 7.64(2H t), 7.60(1H, d), 7.48(1H, s), 7.09-6.99 (4H, m), 6.83–6.80 (4H, m), 6.59(2H, t), 6.32(1H, d), 6.28(1H, d), 6.19(1H, d); FT-IR (KBr) cm$^{-1}$:2054, 1640, 1482, 1125, 748, 578.

## 5. Results and discussion

### 5.1. Electronegativity of ligands

The electron withdrawing abilities of the ligands were measured by the electronegativity (χ), which was estimated from

**Table 1**
The calculated excited energies, dominant orbital excitations and oscillator strength from time-dependent DFT of all complexes.

| Molecular | States | $\lambda_{cal}$/nm | $f$ | Assignments |
|---|---|---|---|---|
| $(ppz)_2Ir(tfmpptz)$ | S | 336 | 0.254 | HOMO-2 → LUMO (90%) |
| | | | | HOMO-3 → LUMO (3%) |
| | | 289 | 0.1968 | HOMO-2 → LUMO+1(84%) |
| | | | | HOMO-3 → LUMO (2%) |
| | T | 398 | 0 | HOMO-2 → LUMO+1(23%) |
| | | | | HOMO → LUMO+1(26%) |
| | | | | HOMO-2 → LUMO+3(10%) |
| $(ppz)_2Ir(fpptz)$ | S | 342 | 0.156 | HOMO-2 → LUMO (92%) |
| | | 281 | 0.2274 | HOMO-2 → LUMO+3(26%) |
| | | | | HOMO → LUMO+4(56%) |
| | | | | HOMO-2 → LUMO+2(7%) |
| | T | 387 | 0 | HOMO-2 → LUMO(35%) |
| | | | | HOMO → LUMO (13%) |
| | | | | HOMO-3 → LUMO (11%) |
| $(ppz)_2Ir(tfmptz)$ | S | 332 | 0.0498 | HOMO → LUMO+1(15%) |
| | | | | HOMO → LUMO+2(77%) |
| | | 266 | 0.1265 | HOMO-2 → LUMO+3(75%) |
| | | | | HOMO-4 → LUMO+2(4%) |
| | | | | HOMO → LUMO+4(5%) |
| | T | 396 | 0 | HOMO → LUMO (78%) |
| | | | | HOMO-1 → LUMO (13%) |
| $(ppz)_2Ir(pybi)$ | S | 394 | 0.0387 | HOMO-1 → LUMO (10%) |
| | | | | HOMO → LUMO (81%) |
| | | 294 | 0.0377 | HOMO-5 → LUMO (67%) |
| | | | | HOMO-6 → LUMO (18%) |
| | | | | HOMO-3 → LUMO+1(6%) |
| | T | 451 | 0 | HOMO-3 → LUMO (41%) |
| | | | | HOMO-2 → LUMO (19%) |
| | | | | HOMO-1 → LUMO (39%) |

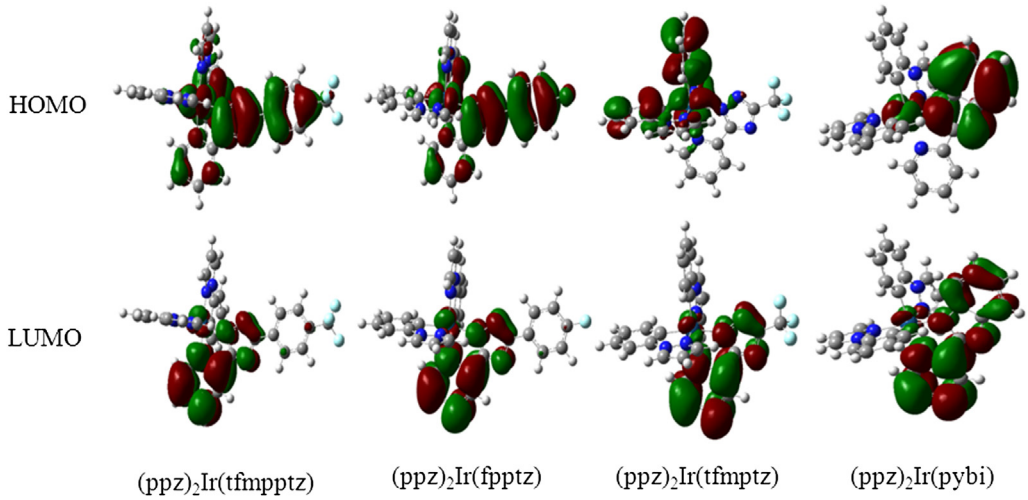


**Fig. 3.** The molecular orbitals characterization of complexes $(ppz)_2Ir(NN)$ from DFT.

the average value of the HOMO (highest occupied molecular orbital) and LUMO (lowest unoccupied molecular orbital) energies: $\chi = -(E_{HOMO} + E_{LUMO})/2$ [18,19]. By optimizing the ligands, the gradually increasing calculated $\chi$ values were Hpybi < Hfpptz < Htfmpptz < Htfmptz, indicating that the electron-withdrawing abilities of the ligands increased along opposite order.

### 5.2. Molecular structures

Single crystals of $(ppz)_2Ir(tfmpptz)$, $(ppz)_2Ir(fpptz)$ and $(ppz)_2Ir(tfmptz)$ were grown from methanol or dichloromethane solution and characterized using X-ray crystallography. Structures are shown in Fig. 1 and selected crystallographic data are provided in experimental section. Three complexes had deformed octahedral coordination geometry around the iridium center with cis- C, C and trans- N, N chelate configuration. The C–C and C–N intraligand bond lengths and angles were within normal ranges. The electron-withdrawing trifluoromethyl group of $(ppz)_2Ir(tfmpptz)$ existed as disorder structure and each fluoro occupied 50%, as shown in Fig. 1a. The average bond lengths of Ir-C were increasing in the order of $(ppz)_2Ir(fpptz)$ (av. 2.000 Å) < $(ppz)_2Ir(tfmpptz)$(av. 2.003 Å) <$(ppz)_2Ir(tfmptz)$ (av. 2.014 Å), indicating that the stronger electron-withdrawing abilities of ancillary ligand resulted in a stronger coordinate field. The bond lengths of the Ir-N (*NN*) in three complexes were longer than those of the $Ir(ppz)_3$. The interaction between $Ir^{3+}$ and N of ppz became stronger relative to $Ir(ppz)_3$ [8]. Additionally, the bond energy of Ir-N became weaker by increasing the conjugation of the ancillary ligand.

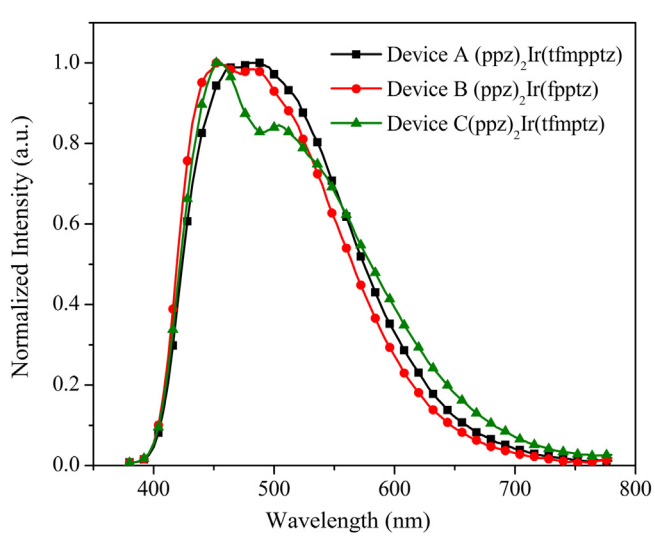


**Fig. 4.** The EL spectra of devices A–C by using $(ppz)_2Ir(NN)$ as dopants (at voltage of 8 V).

### 5.3. Photophysical properties

The absorption and emission spectra of these complexes were recorded in $CH_2Cl_2$ solution at room temperature and were displayed in Fig. 2a. The intense absorption bands at 250–280 nm, were attributed to the ligand-centered $(\pi-\pi^*)^1$ transitions of *NN* ligands. The $(\pi-\pi^*)^1$ bands were accompanied by weaker, lower energy features extending into the visible region from 290 to 350 nm, which was likely associated with single metal-to-ligand charge-transfer ($^1$MLCT) transitions [20]. The absorption bands at about 400 nm were assigned to the triplet MLCT transitions involving the ppz and *NN* ligands and mainly corresponding to the transition from HOMO to LUMO on the basis of time-dependent DFT calculations. The calculated excited energies, dominant orbital excitations and oscillator strength from time-dependent DFT were presented in Table 1.

A close comparison of the emission wavelengths with the structures of these iridium complexes revealed the key feature of these complexes. As shown in Fig. 2a, the emission maximum of $(ppz)_2Ir(tfmpptz)$, $(ppz)_2Ir(fpptz)$, $(ppz)_2Ir(tfmptz)$ and $(ppz)_2Ir(pybi)$ at room temperature appeared at 486, 497, 473 and 530 nm, respectively. The emission spectra of complexes $(ppz)_2Ir(tfmpptz)$ and $(ppz)_2Ir(fpptz)$ with blue-green light emission had red-shifts of 13 and 24 nm relative to $(ppz)_2Ir(tfmptz)$. While, bright-green light was observed for complex $(ppz)_2Ir(pybi)$. The emission colors of these complexes with the same cyclometalating ligands and different *NN* ligands changed from blue to green, and the

**Table 2**
The performances of devices A–C.

| Device | $V_{on}$(V) | $L_{max}$(cd/m$^2$) | $\eta_c$ (cd/A) | $\eta_p$(lm/W) | $\lambda_{max}$ (nm) | CIE |
|---|---|---|---|---|---|---|
| A | 6.4 | 26 487 (11 V) | 6.25 | 1.63 | 480 | (0.23, 0.31) |
| B | 5.9 | 22 278 (13 V) | 5.7 | 1.53 | 453 483 | (0.22, 0.29) |
| C | 7 | 12 142 (13 V) | 7.3 | 2.1 | 453 505 | (0.25, 0.30) |

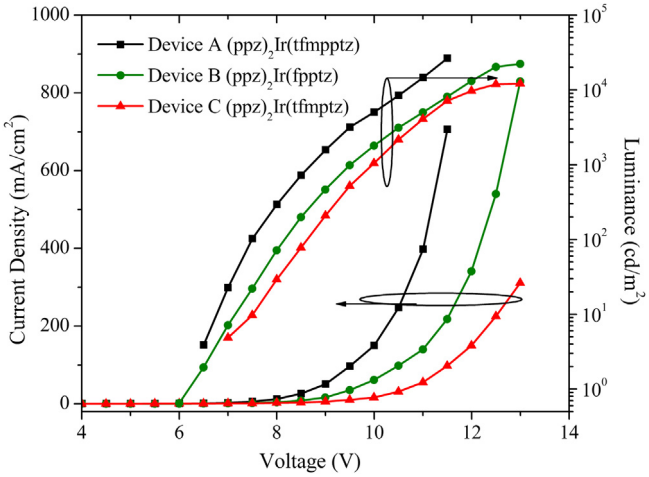


**Fig. 5.** *L–V–J* curves for devices A, B and C.

wavelengths varied by 57 nm. This result provides that the *NN* ligands play a key factor in the emission color of these iridium complexes.

Phosphorescent spectra of $(ppz)_2Ir(fpptz)$ and $(ppz)_2Ir(tfmptz)$ at 77 K were displayed in Fig. 2b. The complex $(ppz)_2Ir(tfmptz)$ show phosphorescent peaks at 426, 452 nm and a shoulder peak at 479 nm. Compared with PL spectra, phosphorescent spectra have obvious blue shift and without fine vibronic progressions. Therefore, the lowest excited triplet states of these complexes are likely to be dominantly the $^3$MLCT excited state [8]. The triplet levels ($E_T$) of $(ppz)_2Ir(fpptz)$ and $(ppz)_2Ir(tfmptz)$, which can be inferred from phosphorescent spectra, are 2.76 and 2.91 eV.

To gain insight into the photophysical behavior of all complexes, DFT was applied to molecular orbital studies. Calculations show that the LUMOs of these complexes were all located on the ancillary *NN* ligands and Iridium atoms, as displayed in Fig. 3. Thus, it would get easy to tune emission color and obtain pure-blue phosphorescent by modification *NN* ligand. On the other hand, HOMOs had the different distributions. The HOMOs of complexes $(ppz)_2Ir(tfmpptz)$ and $(ppz)_2Ir(fpptz)$ had similar plots, which populated on the *NN* and ppz ligands, especially on the *NN* ligand. However, the HOMO and LUMO of $(ppz)_2Ir(tfmptz)$ were located on *NN* and ppz ligands, respectively. The charge transitions became more difficult than $(ppz)_2Ir(tfmpptz)$ and $(ppz)_2Ir(fpptz)$. So the emission of $(ppz)_2Ir(tfmptz)$ exhibited better blue phosphorescent. In the case of complex $(ppz)_2Ir(pybi)$, the HOMO and LUMO all appeared on the *NN* of pybi ligand, suggesting that only *NN* – ligand-based charge transitions had contribution to the excited state (in Fig. 3). This also provides rationale for explaining the observed large red shift of the emission spectra of complex $(ppz)_2Ir(pybi)$.

### 5.4. Electrochemical behaviors

The electrochemical behaviors of these iridium complexes were investigated by cyclic voltammetry. The measured onset oxidation ($E_0^{ox}$) and reduction potentials ($E_0^{red}$) of each complex were used to calculate the HOMO and LUMO levels. The HOMO/LUMO levels of complexes $(ppz)_2Ir(tfmpptz)$, $(ppz)_2Ir(fpptz)$, $(ppz)_2Ir(tfmptz)$ and $(ppz)_2Ir(pybi)$ are −6.01/−3.17, −6.05/−3.26, −6.59/−3.26 and −6.00/−3.34 eV, respectively.

The stronger-electronegativity ancillary ligand Htfmptz resulted in a slightly stabilized HOMO level for complex $(ppz)_2Ir(tfmptz)$. However, one of the key factors affecting the LUMO level in these systems was the degree of conjugation. More effective conjugation of Hpybi stabilized the LUMO for complex $(ppz)_2Ir(pybi)$. The stabilized LUMO level facilitated the electron injection. The energy gaps of complexes $(ppz)_2Ir(tfmpptz)$, $(ppz)_2Ir(fpptz)$, $(ppz)_2Ir(tfmptz)$ and $(ppz)_2Ir(pybi)$ were 2.84, 2.79, 3.33 and 2.66 eV, respectively.

### 5.5. Electroluminescent properties

To character the electroluminescent properties of these complexes, the devices A–C were fabricated by using complexes$(ppz)_2Ir(tfmpptz)$, $(ppz)_2Ir(fpptz)$ and $(ppz)_2Ir(tfmptz)$ as the dopant emitter, respectively. The device A-C structures were ITO/NPB (30 nm)/CBP: $(ppz)_2Ir(NN)$ $(ppz)_2Ir(NN)$ (6%, 30 nm)/BAlq(10 nm)/$Alq_3$(30 nm)/LiF(1 nm)/Al (100 nm). Therein, the $(ppz)_2Ir(NN)$ is $(ppz)_2Ir(tfmpptz)$ (for device A), $(ppz)_2Ir(fpptz)$ (for device B) and $(ppz)_2Ir(tfmptz)$ (for device C), respectively.

The EL spectra of device A was originated from $(ppz)_2Ir(tfmpptz)$ with maximum peak at 480 nm, as can be seen in Fig. 4, indicative of efficient energy transfer from host of CBP to $(ppz)_2Ir(tfmpptz)$. The EL emissions of NPB and CBP are at the range of 400–430 nm [21]. The maximum emission peaks of device B located at 453 and 483 nm and at 505 nm for device C. Therefore, EL spectra of device B

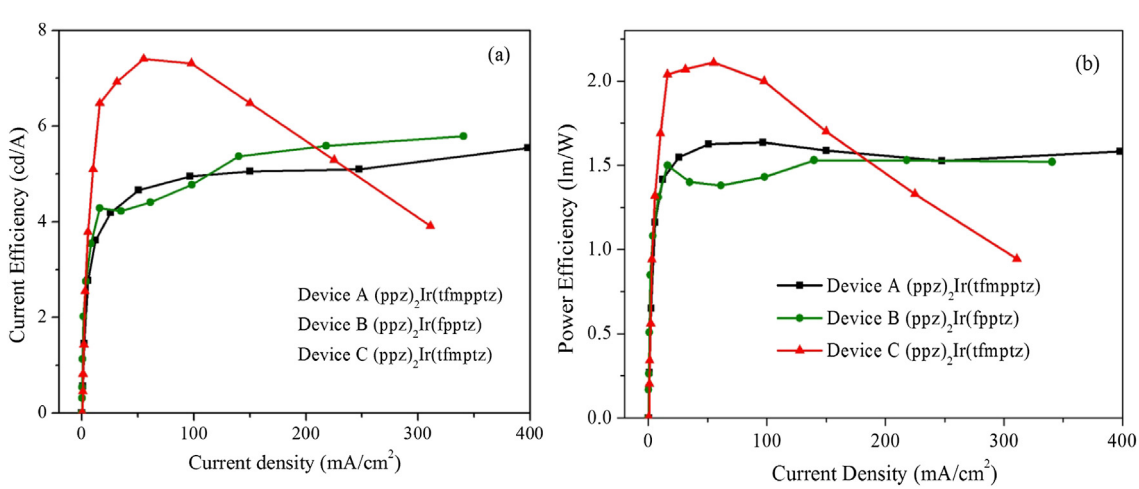


**Fig. 6.** The J-$\eta_c$(a) and J- $\eta_p$(b) curves for devices A, B and C.

and C indicate efficient energy transfer from host to corresponding iridium complexes.

The turn-on voltages (the voltage at a brightness of 1 cd/m$^2$) were 6.4 V for device A, 5.9 V for device B and 7 V for device C. The higher turn-on voltages may be resulted from the high energy barrier between NPB and CBP. Device A had maximum luminance ($L_{max}$) of 26 487 cd/m$^2$, maximum current efficiency ($\eta_c$) of 5.5 cd/A, maximum power efficiency ($\eta_p$) of 1.6 lm/W with CIE coordinates of (0.23, 0.31), as listed in Table 2 and displayed in Fig. 5 and Fig. 6. Both devices A and B showed lower maximum$\eta_c$than device C. But the efficiencies of device C were dramatically decreased with increasing current density. A measure of the roll-off can be defined as the percentage drop in $\eta_{EL}$ at a given field ($F$) or current density ($j$) with a reference to its maximum value of $\eta_{EL}$, that is $roll-off = \eta_{EL}(\max) - \eta_{EL}(F,j)/\eta_{EL}(\max)$, where $\eta_{EL}$ represents current efficiency [22]. The decreased roll-off for device C, 46.5% at 311 mA/cm$^2$, was obvious, which had a maximum $\eta_c$ of 7.3 cd/A. The roll-off for device B was only 1.7% at 539 mA/cm$^2$, significantly lower than device C. Compared with the reported blue-light emitting devices, the efficiencies in this manuscript is much lower due to the mismatched energy levels in devices.

## 6. Conclusion

In summary, four pyrazole complexes that gave blue, green-blue and green phosphorescence were reported by the choice of different ancillary ligand. The stronger electronegativity of ancillary ligand led to a lager energy gap, consequently, blue-shift emission spectra. The PhOLEDs doped with complex $(ppz)_2Ir(fpptz)$ had a better performance with maximum luminance of 26487 cd/m$^2$ and a rather lower efficiency roll-off value. Our investigations show that the subtle change in ligand overcame the roll-off of efficiency. The performances were achieved without optimization for OLED energy level structure. The efficiency of PhOLED doped these Ir(III) complexes could be further improved by optimizing device structure.

## Acknowledgments

This work was financially supported by National Natural Scientific Foundation of China (21071108, 60976018, 21101111, 61205179); Natural Science Foundation of Shanxi Province (2008011008, 2010021023-2); Program for Changjiang Scholar and Innovation Research Team in University (IRT0972).

## References

[1] Gong SL, Fu Q, Wang Q, Yang CL, Zhong C, Qin JG, et al. Adv Mater 2011;23(42):4956–9.
[2] Fan CH, Sun PP, Su TH, Cheng CH. Adv Mater 2011;23(27):2981–5.
[3] Fu HS, Cheng YM, Chou PT, Chi Y. Mater Today 2011;14(10):472–9.
[4] Xia ZY, Xiao X, Su JH, Chang CS, Chen CH, Li DL, et al. Synth Met 2009;159:1782–5.
[5] Yook KS, Lee JY. Adv Mater 2012;24(24):3169–90.
[6] Jeon SO, Jang SE, Son HS, Lee JY. Adv Mater 2011;23(12):1436–41.
[7] Sasabe H, Kido J. Chem Mater 2011;23(3):621–30.
[8] Tamayo AB, Alleyne BD, Djurovich PI, Lamansky S, Tsyba I, Ho NN, et al. J Am Chem Soc 2003;125(24):7377–87.
[9] Yeh SJ, Wu MF, Chen CT, Song YH, Chi Y, Ho MH, et al. Adv Mater 2005;17(3):285–9.
[10] Lu KY, Chou HH, Hsieh CH, Yang YH, Tsai HR, Tsai HY, et al. Adv Mater 2011;23(42):4933–7.
[11] Becke AD. Phys Rev A 1998;38(6):3098–100.
[12] Lee C, Yang WT, Parr RG. Phys Rev B 1988;37(12):785–9.
[13] Yang G, Liao Y, Su Z, Zhang H, Wang Y. J Phys Chem A 2006;110(28):8758–62.
[14] Ran XQ, Feng JK, Ren AM, Tian WQ, Zou LY, Liu YL, et al. J Phys Org Chem 2009;22(7):680–90.
[15] Barone V, Cossi M. J Phys Chem A 1998;102:1995–2001.
[16] Hein DW, Alheim RJ, Leavitt JJ. J Am Chem Soc 1957;79(2):427–9.
[17] Hsieh CH, Wu FI, Fan CH, Huang MJ, Lu KY, Chou PY, et al. Chem Eur J 2011;17(33):9180–7.
[18] Zhan CG, Nichols JA, Dixon DA. J Phys Chem A 2003;107(20):4184–95.
[19] Shi LL, Hong B, Guan W, Wu ZJ, Su ZM. J Phys Chem A 2010;114(24):6559–64.
[20] Li X, Zhang Q, Tu YQ, Ågren H, Tian H. Phys Chem Chem Phys 2010;12:12730–3736.
[21] Li X, Chi HJ, Lu GH, Xiao GY, Dong Y, Zhang DY, et al. Org Electron 2012;13:3138–44.
[22] Cocchi M, Fattori V, Virgili D, Sabatini C, Marco PD. Appl Phys Lett 2004;84:1052–4.